

Phenomenological model for yield stress based on the distribution of chain lengths in a dilute magnetorheological fluid under an oscillatory magnetic field

F. Donado and P. Miranda-Romagnoli

*Instituto de Ciencias Básicas e Ingeniería de la Universidad Autónoma del Estado de Hidalgo-AAMF,
Pachuca 42184, Pachuca, México,
e-mail: fernando@uaeh.edu.mx*

R. Agustín-Serrano

*Facultad de Ciencias Físico Matemáticas, Universidad Autónoma de Puebla,
Puebla 72570, Puebla, México.*

Received 25 April 2012; accepted 16 October 2012

We study the distribution of chain lengths in a magnetorheological fluid based on mineral magnetite particles dispersed in a dextrontype oil exposed simultaneously to a static magnetic field and a sinusoidal field of low amplitude, the fields are transverse to each other. We experimentally determined the general behavior of the distributions under several conditions of intensities of the fields, particle concentration, liquid viscosity, and frequency of the sinusoidal field. We found that in all cases exponential fits describe well these distributions. Based on this result we propose a simple yield stress model for a magnetorheological fluid which differs from other models that posit all chains are of the same length. We compare this model with experimental results and found that there is a well qualitative agreement with them and in some cases also there is a quantitative agreement. In the case of using only static field, the model is in accord with the existence of a magnetic field threshold above which the yield stress increases faster than below it.

Keywords: Magnetorheological fluids; yield stress; chain length distribution.

PACS: 83.80.Gv; 83.60.La; 83.60.Np

1. Introduction

The main characteristic of a magnetorheological fluid (MR fluid) is that notable changes in its physical properties can be induced and tuned reversibly by applying magnetic fields [1-10]. They are used in novel adaptive dampers in cars and buildings and also in optical finishing of lenses [11-14]. MR fluids are composed of magnetizable microparticles dispersed in a liquid of low viscosity like mineral oil, silicon oil, or water, as well as other liquids. When a magnetic field is turned on, particles interact with each other and form elongated aggregates oriented in the direction of the applied field. The characteristics of the aggregates are sensibly dependent of both magnetic field and particle concentration. Such characteristics, in turn, determine the physical property changes in MR fluids [3,5,7-10,15]. In the low particle concentration regime, the structures formed by the particles are chains, commonly one particle wide. For medium and high particle concentrations, the aggregates are fibrous; they are formed by intertwined chains [16]. In MR fluids with low particle concentration, the chains formed by the particles share some characteristics with those formed in systems like polymers and gels. Thus, studies in MR fluids can be used for modelling a wide variety of similar systems due to the fact that particle interactions can be tuned by the intensity of the magnetic field [17,18].

For modelling the rheological behavior of an MR fluid, it is necessary to determine interactions among chains and among these with their surroundings, these includes the liquid where they are dispersed and the walls that produce the

shear stress [1]. Therefore chain characteristics are an important aspect to take into consideration. In most Refs. 8, 10, and 19 to 22, it is commonly assumed that the system is formed by an ensemble of ordered chains of the same length. However, images coming from many different experiments show that chain lengths are not of the same size; in fact, there is a wide distribution of chain lengths [7,9,17,18,23,24]. To describe the MR fluid structure, there is only one case where chains are of the same length: when the gap between plates is much shorter than the average chain length. If the plate separation is wider than the average chain length, then the distribution of chain lengths must be taken into consideration when modelling physical property changes induced by magnetic fields. This is the case when it involves a system with low particle concentration under magnetic fields of low intensity.

In Ref. 25 we studied the average chain length in a quasi-two-dimensional system. It was found that average chain length is dependent on primary parameters and is well described by power laws; however, it was not presented a study of the distribution of the chain lengths. In this work we are continuing the study of the same system. In Sec. 2, we describe the experimental setup. In Sec. 3 we present a comprehensive analysis of experimental data to determine the distributions of the chain lengths. In Sec. 4 we develop a simple model for yield stress based on both chain length distributions and power laws for the average chain length; the model is compared with experimental data. Finally, in Sec. 5, we give some comments and conclusions.

2. Experimental setup

The process of obtaining chain lengths has been described elsewhere [25,26]. In brief, an MR fluid was prepared using micrometric particles of $65 \mu\text{m}$ with a standard dispersion of $15 \mu\text{m}$ and a density of 5.1 g/cm^3 . The particles were dispersed in a Dexrontype oil of viscosity 76 cP . A sample of this dispersion was poured into a rectangular cell 14 mm in width, 19 mm in length. The MR fluid sample was exposed simultaneously to a static field and to a sinusoidal field of low amplitude that is considered a perturbation. These fields are horizontal and orthogonal to each other and were produced by using Helmholtz coils located around the cell. In most of the experiments, the r.m.s. amplitude of the sinusoidal field was 15% of the static field. The particle concentration is indicated by the parameter ϕ , the fraction of surface area occupied by the particles; in most of the experiments $\phi = 0.05$. The sample was illuminated using transmitted light. The aggregation process was observed using a Meiji EMZ-TR microscope during 200 s , starting when the fields were turned on; the final stage, when the fields were turned off, was recorded using a Diagnostic Instruments digital camera adapted to a microscope. The optical observation field only spanned a quarter of the cell, thus four photos were taken and joined in order to span the whole cell. These photos were digitally treated to enhance the contrast between the dark areas corresponding to the particles, and the clear areas corresponding to the liquid. The chain lengths were determined using the software Sigma Scan Pro 4.0.

To measure yield stress we used a rotational rheometer Bohlin CVO 120 HR in a controlled-stress mode. It had a plate-plate geometry with a diameter of 55 mm of non-magnetic material. The temperature was steady at 20°C by means of a Peltier control. The MR fluid sample was exposed simultaneously to a combination of a static magnetic field and a low amplitude sinusoidal field, transverse to one another. To generate the static field a solenoid was used and to generate the sinusoidal field a Helmholtz coil was used.

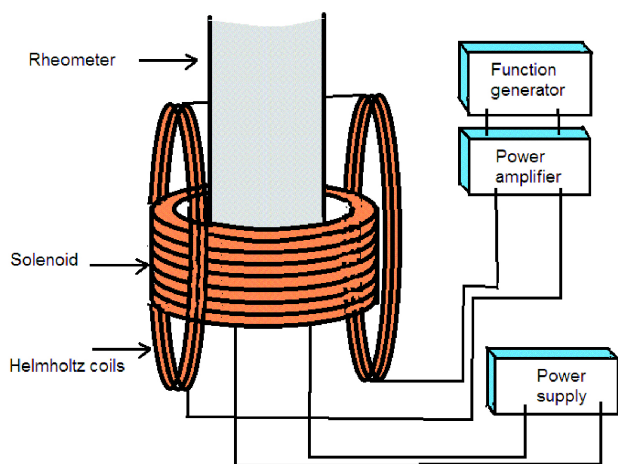


FIGURE 1. Scheme of the experimental setup to determine rheological properties.

This coil was fed by an amplifier circuit powered by a function generator Elenco GF8056. Figure 1 shows a scheme of the setup used to determine yield stress.

3. Chain length distributions

Figure 2 shows a view of a typical ensemble of chains. Although a small fraction of particles are isolated, most of them form chains of different lengths; the shorter chains being more numerous than the longer ones. Figure 3 shows four histograms corresponding to the same data, for different step thickness. It was observed that all of them exhibit an exponential behavior. Hereinafter we construct the histograms using ten bins. We determined the distribution of chain lengths for several conditions of magnetic fields, particle concentration and liquid viscosity. We found that the distributions of these series show an exponential behavior of the form

$$f(l) = A_e \exp(-\alpha l) \tag{1}$$



FIGURE 2. Typical ensemble of chains in a dilute MR fluid under a magnetic field of low intensity.

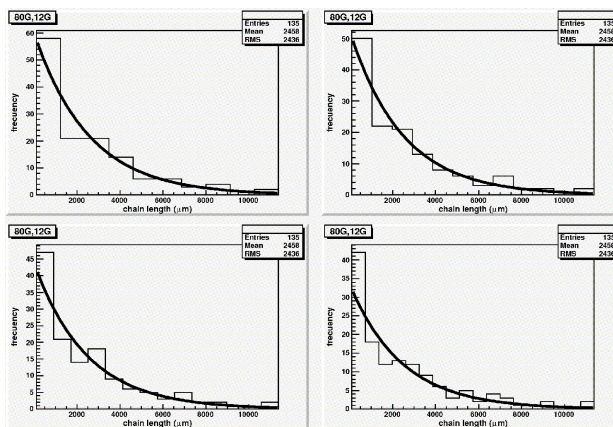


FIGURE 3. Comparison of histograms for the same data, in each one it was used different number of bins 10, 12, 14 and 18, corresponding to different step thickness.

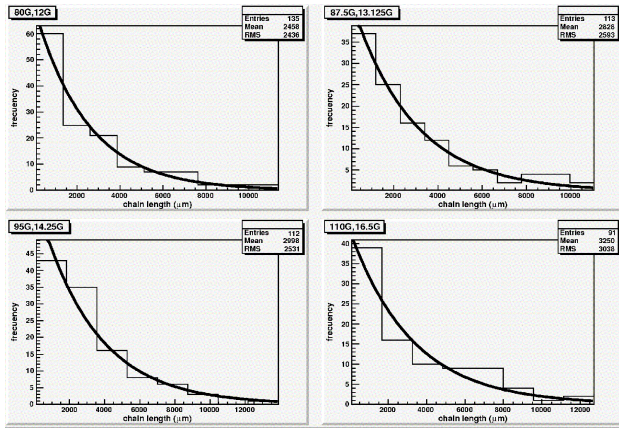


FIGURE 4. Typical histograms for different values of the magnetic fields, the ratio between the r.m.s sinuidal field amplitude and the static field is 15%.

where A_e and α must be functions of the experimental parameters: the magnetic field, particle concentration, liquid viscosity, and so on. In the following paragraphs, we show in detail these distributions.

In order to determine the distributions of chain lengths for different magnetic field intensities, we carried out a series of experiments where both fields were varied but maintaining a ratio of 15 % between them. Figure 4 shows some selected histograms corresponding to different values of the magnetic fields. To compare the changes induced by the magnetic fields on the distribution, we determined the rate of change α of each exponential distribution and then they were compared. Figure 5 shows the parameter α as a function of the magnetic field intensity. It was observed that the rate of change decreased as the magnetic field increased. For this series, the parameter α is a linear function of the magnetic field as can be observed in Fig. 5. As the magnetic field intensity increases, the number of the chains decreases because the distribution moves toward longer chains.

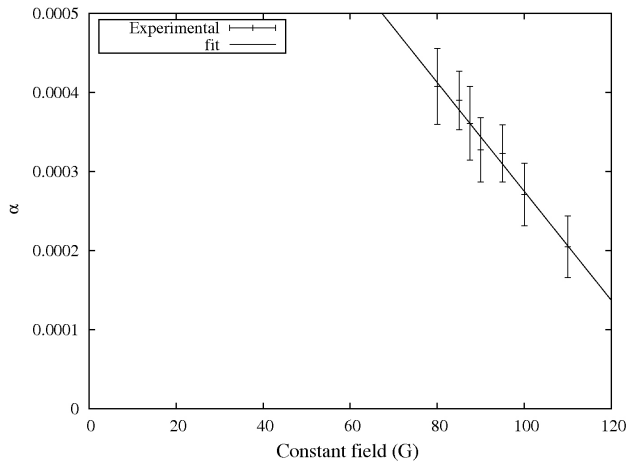


FIGURE 5. Parameter α as a function of the static magnetic field intensity for the series where both fields are varied and the ratio between them is 15 %.

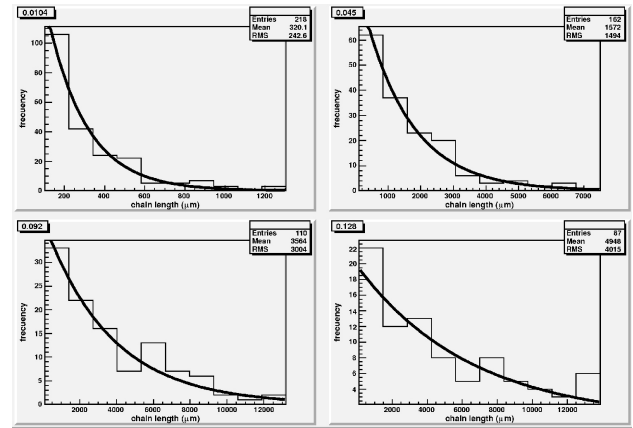


FIGURE 6. Typical histograms corresponding to different values of particle concentration.

The changes on distributions of chain lengths induced by variations of the particle concentration are especially interesting because chain characteristics change qualitatively very quickly, as particle concentration grows. We carried out a series of experiments where particle concentration was varied, but always in the low particle concentration regime. When only a static field is applied, particles form chains if the concentration ϕ is below about 0.12. For higher particle concentrations, aggregates with an interconnected structure are formed. In the case of applying both fields, it is more difficult to establish a particle concentration where only chains are formed; beyond $\phi = 0.076$, aggregates with an interconnected structure are formed, this is because the sinusoidal field promotes the lateral aggregation. In both cases there are no well-defined limits to the formation of chains. Aggregates with an interconnected structure still can be characterized by its length; that is why we consider them in our analysis. Figure 6 shows some typical histograms of chain lengths for different values of the particle concentration in cases where both fields were applied. Again, the distributions can be described by exponential functions in all the range of particle concentration that we explored.

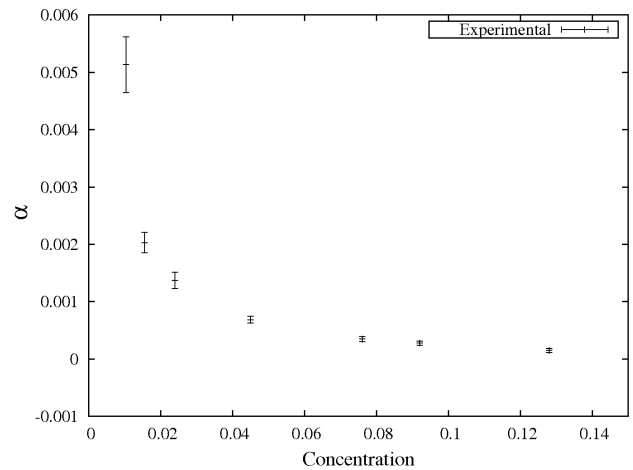


FIGURE 7. Parameter α as a function of the particle concentration.

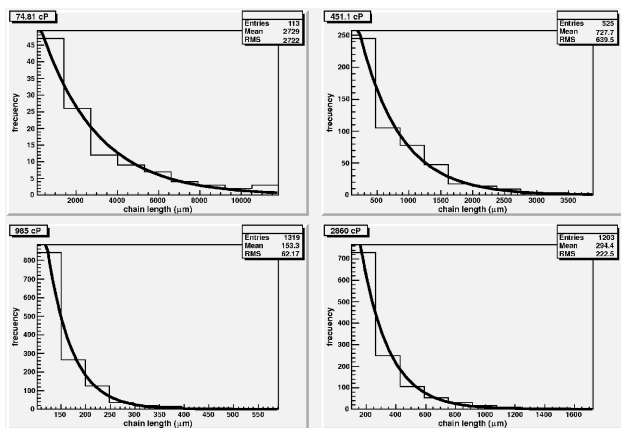


FIGURE 8. Typical histograms corresponding to different values liquid viscosity.

Figure 7 shows the general behavior of the parameter α as a function of the particle concentration. As the particle concentration increases, long chains are formed faster and more frequently than for lower particle concentrations; thus α decays very quickly as the particle concentration increases. Therefore, the difference in frequency of consecutive intervals in the distributions of chain lengths becomes smaller as the particle concentration increases.

The liquid viscosity is another important parameter because it determines some aspects of the dynamics of chains, especially the speed of aggregation which in turn determines the chain lengths. Figure 8 shows histograms for the chain lengths for different samples of MR dispersions prepared using Cannon viscosity standards which differ among them in their viscosity. Figure 9 shows the general behavior of the parameter α as a function of the liquid viscosity. For this series we did not observe a clear general trend mainly because of the low number of points. Except for a measurement corresponding to a liquid viscosity of 900 cP, the other points could be fitted in a first approximation by using a linear function.

Figure 10 shows some distributions of chain lengths corresponding to the series where different frequencies of the

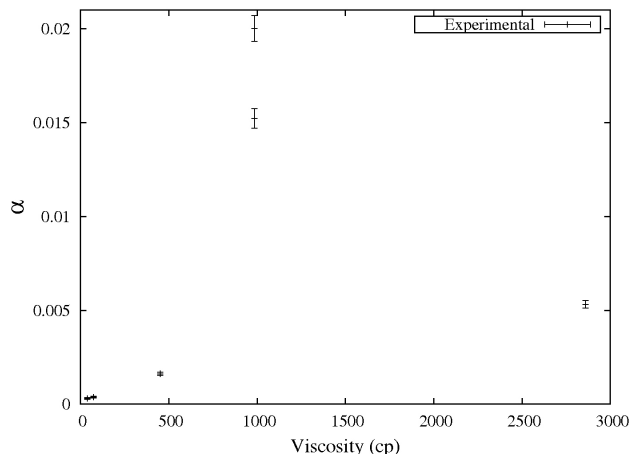


FIGURE 9. Parameter α as a function of the liquid viscosity.

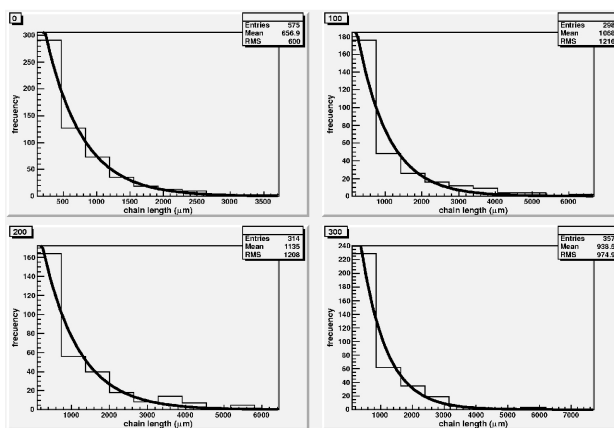


FIGURE 10. Typical histograms corresponding to the series where different perturbation frequencies are applied.

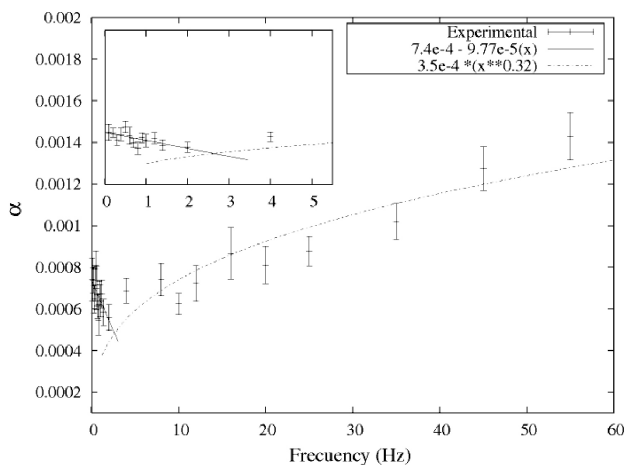


FIGURE 11. Parameter α as a function of the perturbation frequency.

perturbation have been applied. It was observed again, as in the previous series of experiments, that exponential functions fit well with these distributions. Figure 11 shows the general behavior of the parameter α as a function of the perturbation frequency. This graph differs from the previous ones because it was observed two frequency regimes of qualitatively different behavior. In the first regime, α decreases while in the second it increases, as the perturbation frequency increases. This behavior is in accord with the behavior of the average chain length previously studied in Ref. 25.

As we have shown, all distributions of chain lengths are well described by exponential distributions of the form expressed by Eq. (1). This result is in accord with theoretical results [17,27-29]. To determine the explicit dependencies, we proposed the following construction. We started with an approximation for the total number of particles N , that is

$$N = \int_0^{\infty} A_e l \exp(-\alpha l) dl = \frac{A_e}{\alpha^2}. \quad (2)$$

Thus $A_e = N\alpha^2$. Similarly the total number of chains N_c can be written as

$$N_c = \int_0^\infty N \alpha^2 \exp(-\alpha l) dl = N \alpha. \quad (3)$$

From here $\bar{L} = N/N_c = 1/\alpha$. In a volume V_T of a MR fluid composed of spherical particles of radius a the total number of particles N is given by

$$N = \frac{3\phi_v V_T}{4\pi a^3}. \quad (4)$$

where ϕ_v is the fraction of volume occupied by particles. Thus

$$\alpha = \frac{1}{\bar{L}} \quad (5)$$

$$A_e = N\alpha^2 = \frac{3\phi V_T}{4\pi a^3 \bar{L}^2}. \quad (6)$$

These results are in agreement with the theoretical result proposed in Ref. 27.

To find the dependencies of α and A_e on other variables, let us use previous results from Ref. 25; that is, we use the fact that the average chain length follows power laws. For low frequencies it was found that

$$\bar{L}(X_i) = A f_p^{\delta_i} \phi^{x_i} \eta^\psi t^\alpha H_b^\theta, \quad (7)$$

where $\delta_i = 0.07 \pm 0.02$, $\xi = 1.06 \pm 0.03$, $\psi = -0.57 \pm 0.04$, $\alpha = 0.53 \pm 0.01$, and $\theta = 1.48 \pm 0.14$. Therefore, through these power laws, and Eqs. 5 and 6, it is possible to describe the chain length distributions, Eq. (1), as functions of the main measurable parameters that describe the system.

From Eq. (5), a very simple relation was observed between the average chain length and the rate of change of the exponential distribution: they are inversely proportional to each other. In order to determined whether or not experimental data were in accord with this result, Figs. 12, 13, 14 and 15 show the parameter α as a function of the inverse of average chain length when the intensities of the fields, particle concentration, liquid viscosity and perturbation frequency are varied, respectively. In each figure, the dotted line has a slope equal to unity representing the prediction of the model. In the case where the field intensities were varied, in the Fig. 12 it is observed that there is a linear relation, however the slope of the line is different from unity as was expected. It is observed that the model agrees well with the experimental data mainly in the middle of the magnetic field range that we studied, around 80 G.

From the Fig. 13, corresponding to the series where particle concentration is varied, it can be observed a good qualitative agreement between theory and experimental data; that is, there is a linear fit and its slope is close to unity. The behavior of α , as a function of the liquid viscosity, is shown in Fig. 14; however, in this case it is not easy to find a general trend because there are a small number of experimental data.

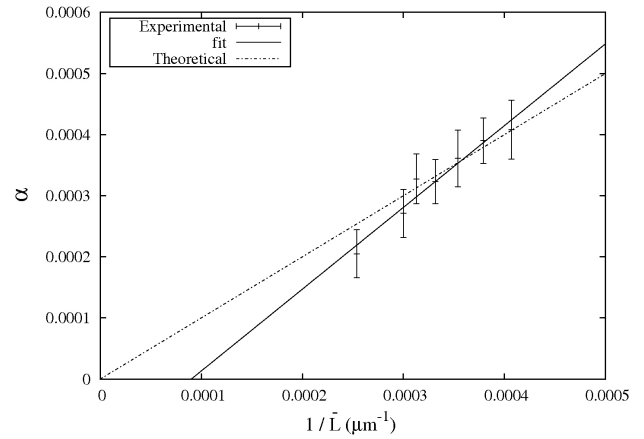


FIGURE 12. Parameter α as a function of inverse of the average chain length, for the case of varying magnetic field.

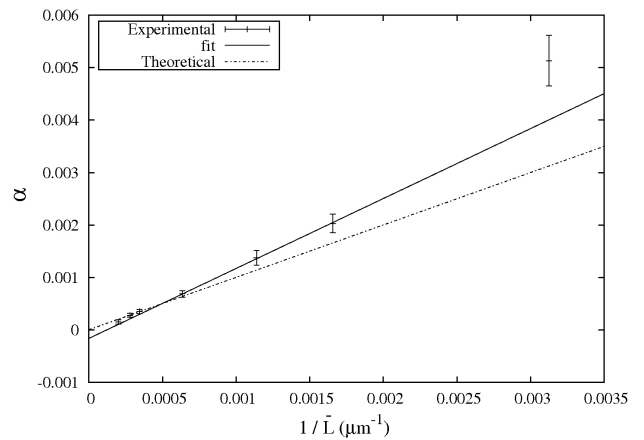


FIGURE 13. Parameter α as a function of inverse of the average chain length, for the case of varying particle concentration.

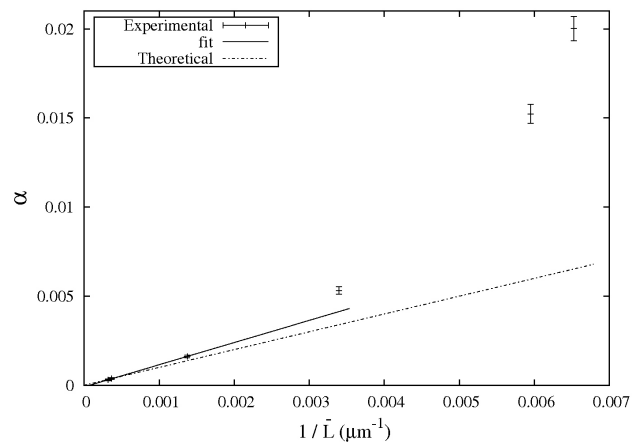


FIGURE 14. Parameter α as a function of inverse of the average chain length, for the case of varying liquid viscosity.

Finally, in Fig. 15 is showing the general trend of the parameter α behavior as a function of the inverse of average chain length corresponding to the series when the frequency is varied. The linear behavior of the data also was observed;

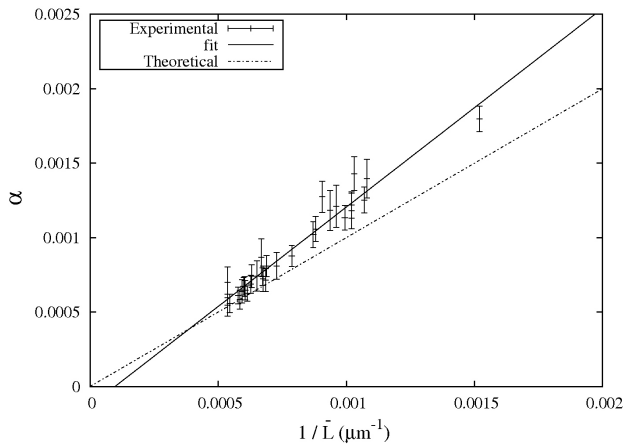


FIGURE 15. Parameter α as a function of inverse of the average chain length, for the case of varying perturbation frequency.

although, the slope differs from unity. This is interesting because the trend of α as a function of perturbation frequency shows two different behaviors.

4. A simple yield stress model

In a static yield stress measurement, the sample is exposed to increasingly higher values of shear stress. The aim is to determine the stress when the system begins to flow. This stress value is the static yield stress. To measure yield stress, a rotational rheometer with a parallel plates geometry and functioning in the controlled stress mode can be used, although it is not the only method that can be used to determine yield stress. Accordingly to the Refs. 8 and 27, the shear stress τ is the product of the surface density of chains ρ_s that span the gap between the plates and the restoring force \mathbf{F}_r produced by a chain under the shear stress.

$$\tau = \rho_s F_r. \quad (8)$$

In our system we have shown that the distributions of the chain lengths are decay exponentials in all cases, thus only a fraction of the total chains are long enough to span the plates. These chains resist to deforming due to shear stress; thus the system too. These chains determine the static yield stress. Taking into consideration the distribution of the chain lengths, expressed by the Eq. (1), the fraction of particles that could form bonds between the plates, $\Phi(\bar{L})$, can be obtained by

$$\begin{aligned} \Phi(\bar{L}) &= \frac{\int_0^{\infty} N \alpha^2 l \exp(-\alpha l) dl}{\int_0^{\infty} N \alpha^2 l \exp(-\alpha l) dl} \\ &= \left(\frac{h}{\bar{L}} + 1 \right) \exp\left(-\frac{h}{\bar{L}}\right). \end{aligned} \quad (9)$$

Therefore, the number of particles that form chains long enough to span the plates, $N_p = N\Phi(\bar{L})$, where N is given by Eq. (4), is given by

$$N_p = \frac{3\phi_v Ah}{4\pi a^3} \Phi(\bar{L}), \quad (10)$$

where we have used $V_T = Ah$, being A the plate area. A similar proposal was taken in Ref. 27, although the authors used an analytical expression for the average chain length that produced different results. With N_p particles it is possible to form $N_p/(h/2a)$ chains spanning the plates. Finally, the surface density of chains is given as

$$\rho_s = \frac{3\phi_v}{2\pi a^2} \left[\left(\frac{h}{\bar{L}} + 1 \right) \exp\left(-\frac{h}{\bar{L}}\right) \right]. \quad (11)$$

In this result it is observed that chain length distribution is a function of the average chain length \bar{L} and through this quantity the distribution is a function of particle concentration, magnetic fields, liquid viscosity and time.

On other hand, the restoring force \mathbf{F}_r of a chain under shear stress is the tangential component of the magnetic force [8]. The magnetic force among particles is due mainly to dipole moments induced in the particles when the magnetic field is turned on. The magnetic force, expressed in polar coordinates, between a pair of particles is given by

$$\begin{aligned} \mathbf{F}_m &= -\frac{3\mu_0}{4\pi m^2} \frac{1}{r_{ij}^4} \\ &\times \left[(3 \cos^2 \theta - 1) \hat{r}_{ij} + (\sin(2\theta)) \hat{\theta} \right]. \end{aligned}$$

Because the dipolar interactions decay quickly, in a chain of particles the main contribution to the magnetic force is due to the closest neighbors. Therefore, the restoring stress, is defined as $F_r = \mathbf{F}_m \cdot \hat{\theta}$, is

$$F_r = -\frac{3\mu_0 m^2}{4\pi} \sin(2\theta) \frac{1}{(2a)^4}. \quad (12)$$

The negative sign indicates that the restoring force opposes the deformation. Thus, the restoring force depends on the magnetic moment, particle radius and the angle formed by the chains with respect to the direction of the magnetic field. When the chains are exposed to a shear stress in a direction perpendicular to the static field, they are deformed at an angle inclined with respect to the direction of the magnetic field. It can be shown that only for a certain range of angle values the magnetic interactions are attractive and after a critical angle θ_c the interactions become repulsive and as a consequence the chains are broken at some point and the system begins to flow. The yield stress τ_0 is the shear stress value high enough to produce chain ruptures and consequently to produce a flow. Various studies have calculated the critical angle, one of them proposing that $\tan \theta_c = \sqrt{1/2}$, therefore $\theta \approx 35.26^\circ$ [8].

Using Eqs. (8), (11), (12), the value of the critical angle and the magnetic moment in terms of the magnetization, we obtain a general expression for the magnitude of the shear stress as follows:

$$\tau_0 = \frac{\phi_v \mu_0 \chi_p^2 \sin(2\theta_c) H_{ef}^2}{8} \left[\left(\frac{h}{\bar{L}} + 1 \right) \exp\left(-\frac{h}{\bar{L}}\right) \right]. \quad (13)$$

The difference between Eq. (13) and the proposals by other authors is the term within brackets, which corresponds to the effective fraction Φ of particles that form bonds through the gap.

The effective field applied to our system has two components: a static field in a direction transverse to the flow, with magnitude H_s and a sinusoidal field perpendicular to the static field, with amplitude H_p and frequency f_p . Thus, in our case, the effective field has the following form:

$$\mathbf{H}_{ef} = H_s \hat{j} + H_p \sin(2\pi f_p t) \hat{i}, \quad (14)$$

where t is the time. Thus the yield stress can be written as

$$\begin{aligned} \tau_0 &= \frac{\phi_v \mu_0 \chi_p^2 \sin(2\theta_c)}{8} \left(H_s^2 + \frac{H_p^2}{2} \right) \\ &\times \left[\left(\frac{h}{\bar{L}} + 1 \right) \exp\left(-\frac{h}{\bar{L}}\right) \right], \end{aligned} \quad (15)$$

where the magnitude of \mathbf{H}_{ef} has been obtained from Eq. (14) and $H_p \sin(2\pi f_p t)$ has been changed to its root mean square $H_p/\sqrt{2}$.

Therefore, we have an expression for τ_0 as a function of the average length of aggregates and the amplitudes of the fields. Because \bar{L} is very sensitive to the presence of the sinusoidal field, it is expected that the yield stress can be enhanced by using a perturbation field.

Let us begin by substituting the values of the constants $\mu_0 = 1.26 \times 10^{-6}$ H/m, $\chi_p = 2.17$, $\phi_v = 0.05$, and the value of the critical angle in Eq. (15). We obtain an expression for the yield stress given by

$$\begin{aligned} \tau_0 &= 2.21 \times 10^{-4} \left(H_s^2 + \frac{H_p^2}{2} \right) \\ &\times \left[\left(\frac{h}{\bar{L}} + 1 \right) \exp\left(-\frac{h}{\bar{L}}\right) \right]. \end{aligned} \quad (16)$$

where an additional factor of $[1000/4\pi]^2$ was introduced in order to use the intensity of the field in G units. Equation (20) predicts that τ_0 depends directly on the magnetic field, the separation between the plates, and the average length of the aggregates. According to the Eq. (7), the average length of the aggregate \bar{L} can be expressed as a product of power laws of the variables H_s , H_p , f_p , ϕ , η and t ; thus, τ_0 can be expressed as a function of the same variables, in addition to the dependency on plate separation.

The average length of chains \bar{L} as a function of static field, when $\phi = 0.05$, $\eta = 0.075$ Pa·s and $t = 200$ s, has the following form [25]:

$$\bar{L} = 1.94 H_s^{1.33}, \quad (17)$$

\bar{L} is given in μm and H_s in G. Substituting Eq. (17) in Eq. (19), replacing the value of $h = 3000 \mu\text{m}$ and removing the term corresponding to the oscillating field, it is obtained that

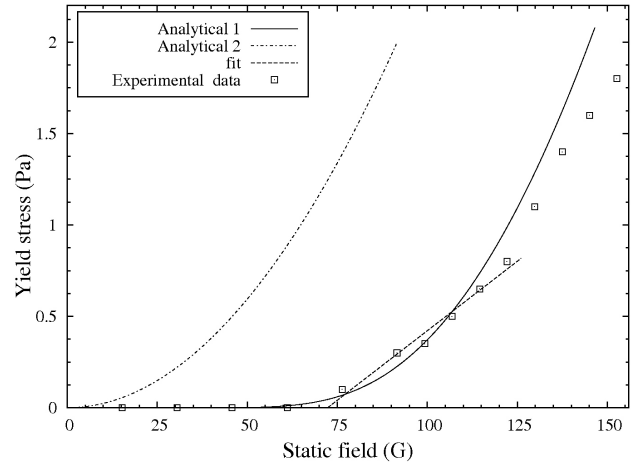


FIGURE 16. Yield stress as a function of the static field in a sample of MR fluid based on mineral magnetite. The solid line is the theoretical behavior according to the model.

$$\begin{aligned} \tau_0 &= 2.21 \times 10^{-4} H_s^2 \left(\frac{1546.39}{H_s^{1.33}} + 1 \right) \\ &\times \exp\left(-\frac{1546.39}{H_s^{1.33}}\right). \end{aligned} \quad (18)$$

Equation (18) represents the behavior of yield stress as a function of the static field only. Figure 16 shows the τ_0 behavior modeled by Eq. (18) (see continuous line). It is noted that in the regime of values below 150 G, the model agrees well with experimental data. In particular the model is in accord with the existence of a threshold magnetic field below which τ_0 is negligible and above which τ_0 grows rapidly. The dotted line represents the behavior of the yield stress when the chain length distribution is not taken into consideration, its behavior scales with the square of the field. It is observed that in the low magnetic field regime the disagreement is greater. In this regime is where our work improves the knowledge of MR fluids.

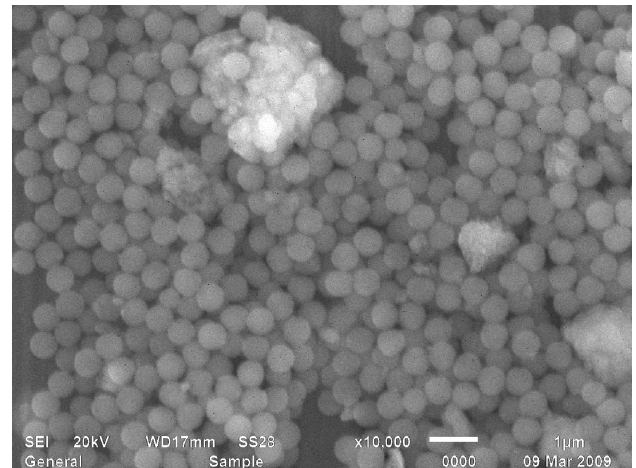


FIGURE 17. SEM photograph of the silica-coated magnetite particles.

We have also conducted experiments using silica-coated magnetite particles. The magnetite particles were obtained by the following chemical reaction in aqueous media: $\text{FeCl}_2(\text{H}_2\text{O})_4 + \text{FeCl}_3(\text{H}_2\text{O})_6 + \text{HCl} + \text{NH}_4\text{OH} + \text{H}_2\text{O} \rightarrow \text{Fe}_3\text{O}_4 + \text{subproducts}$. The characteristic shape of the material was determined from the photographs obtained by SEM. Agglomerates of several sizes, between 0.05 and 15 μm , were observed. In order to coat the magnetite with silica, a dispersion of 200 mg of magnetite, 15 ml of ethanol, and 5 ml of deionized water was shaken by using an ultrasonic bath of 10 minute duration. A mix of 4 ml de TEOS (Tetraetil-orthosilicate) in 30 ml of ethanol was poured into the solution at room temperature. Particles with spherical shape and very homogeneous in size were obtained with this procedure; their density was estimated to be 3.48 g/cm^3 and the average particle diameter was 0.48 microns, with a dispersion of 0.05 microns. Figure 17 shows a SEM photograph of the particles.

In yield stress measurements using this kind of particles, we have observed a behavior similar to what we observed using particles used in Ref. 25. Of course the laws that describe the general trend of the average length of the aggregates are different. Also the magnetization could be different, thus for a more general case it is possible to propose the following general form for yield stress for a dilute dispersion and under low magnetic fields

$$\tau_0 = AH_{ef}^2 \left[\left(\frac{Bh}{HC} + 1 \right) \exp \left(-\frac{Bh}{HC} \right) \right], \quad (19)$$

where A, B, C are unknown constants. This equation predicts that τ_0 depends directly on the magnetic field and separation between the plates. Figure 18 shows the comparison between yield stress measurements and the model given by Eq. (19). It is observed the fitting curve considering A and B as unknown

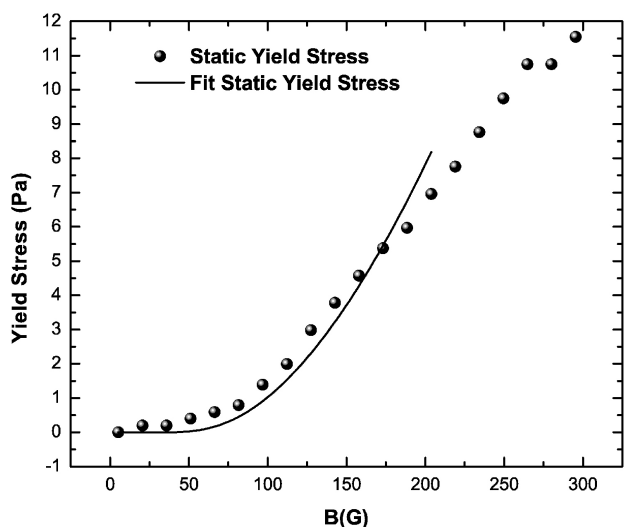


FIGURE 18. Comparison between experimental measurements and theoretical model in a sample of MR fluid based on submicrometric particles of silica-coated magnetite. In this case C was considered as a known parameter and A and B as unknown parameters.

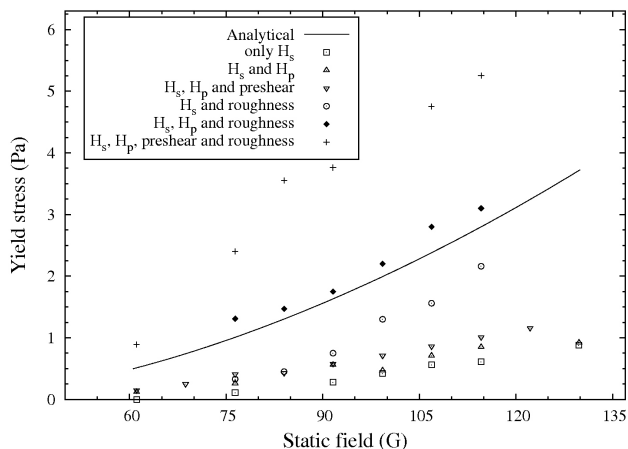


FIGURE 19. Yield stress behavior under presence of different conditions with $H_s = 91.60 \text{ G}$ and $H_p = 0.15H_s$ at 4 Hz.

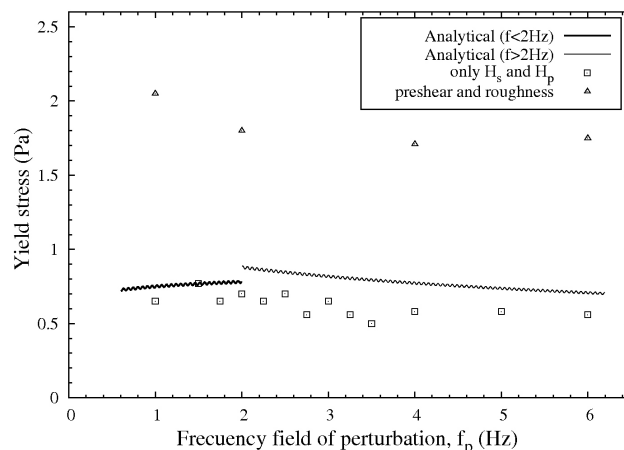


FIGURE 20. Yield stress under a static field of 91.60 G and a variable frequency field with 18.80 G of amplitude.

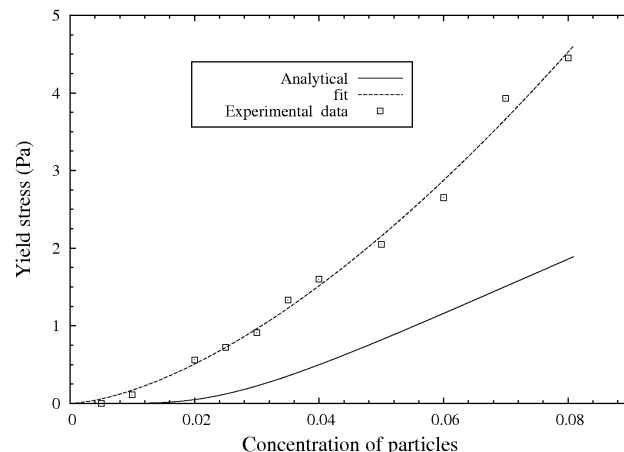


FIGURE 21. Yield stress dependence on the concentration of particles.

parameters and C as known parameter, being the same as in Eq. (17).

The fit is in accord with yield stress measurements and indicates that there exist a magnetic field threshold, around

75 G, above it the yield stress grows faster as the magnetic field increases.

Figures 19, 20 and 21 show the yield stress behavior when the sinusoidal field, considered as a perturbation, is applied. In each graph, the solid line is the theoretical behavior according to our model, Eq. (19). It is observed that there is a qualitative agreement with experimental data; however the model gives larger values for yield stress than those obtained experimentally. If the system is subjected to a shear field before the measurement of yield stress, the agreement is much better. Thus, it seems that in a confined condition like in which the yield stress is measured, the perturbation field acts better over the particle aggregation if a shear field is present. The graphs also indicate that when roughness in the plates are used, the yield stress is enhanced even more. We are working on improving our yield stress model to include the effects of applying a shear field before taking the yield stress measurement and to include roughness in the plate-plate geometry used in the rheometer.

5. Comments and remarks

We have shown a study of chain length distributions and based on our findings we propose a simple model for yield

stress in an MR fluid subjected to an effective oscillating magnetic field. We have shown that chain length distributions are well described by exponential distributions. Based on this result, we propose a simple model for yield stress that qualitatively agrees with some general trends in yield stress. In particular, the agreement of the model with experiments in the case when only a static field is used is very good, at least for low magnetic fields. In the case of using only the static magnetic field, it is worthy of note that model predictions are consistent with the existence of a threshold magnetic field that separate two regions. In the first, the yield stress grows very slowly as the magnetic field increases. In the second, the yield stress grows faster as the magnetic field increases above the threshold magnetic field. This agreement is possible only because our model takes into consideration that chain lengths form a decay exponential distribution. This approach can be used to study similar systems like electrorheological fluids and ferrofluids under low fields presence.

Acknowledgments

The partial financial support by CONACyT, México grant 80629 is acknowledged. R. Agustín-Serrano received a fellowship from CONACyT.

-
1. H. M. Laun, C. Gabriel, and C. Kieburg, *Rheol. Acta* **50** (2011) 141-157
 2. J. Rodríguez-López, L. Elvira Segura, and F. Montero de Espinosa Freijo, *J. Magn. Magn. Mater.* **324** (2012) 222-230
 3. M. Ocalan and G. H. McKinley, *Journal of Intelligent Material Systems and Structures* January (2012) doi: 10.1177/104538911429601
 4. F. Vereda, J. de Vicente, J. P. Segovia-Gutiérrez, and R. Hidalgo-Alvarez, *J. Phys. D: Appl. Phys.* **44** (2011) 425002
 5. J. de Vicente, J. A. Ruiz-López, E. Andablo-Reyes, J. P. Segovia-Gutiérrez, and R. Hidalgo-Alvarez, *J. Rheol.* **55** (2011) 753
 6. M. J. Hato, H. J. Choi, H. H. Sim, B. O. Park, and S. S. Ray, *Colloids and Surfaces A: Physicochem. Eng. Aspects* **377** (2011) 103-109
 7. G.K. Auernhammer, D. Collin, and P. Martinoty, *J. Chem. Phys.* **124** (2006) 204907
 8. J. de Vicente, M.T. López-López, J.D.G. Durán, and F. González-Caballero, *Rheol. Acta* **44** (2004) 94-103.
 9. D. Kittipoomwong and D.J. Klingenberg, and J.C. Ulicny, *J. Rheol.* **49** (2005) 1521.
 10. R. Tao, *J. Phys.: Condens. Matter.* **13** (2001) R979.
 11. N. Caterino, M. Spizzuoco, and A. Occhiuzzi, *Smart. Mater. Struct.* **20** (2011) 065013
 12. M. M. Rashid, N. A. Rahim, M. A. Hussain, and M.A. Rahman, *IEEE Trans. Ind. Appl.* **47** (2011) 1051-1059
 13. P. Horvath and D. Torocsik, *Mechatronics* (2012) 89-93 doi: 10.1007/978-3-642-23244-2-11.
 14. J. C. Lambropoulos, C. Miao, and S. D. Jacobs, *Optics Express* **18** (2010) 19713.
 15. J. de Vicente, D. J. Klingenberg, and R. Hidalgo-Alvarez, *Soft Matter* **7** (2011) 3701-3710.
 16. J.L. Carrillo, F. Donado, and M.E. Mendoza, *Phys. Rev. E* **68** (2003) 061509.
 17. J.M. Tavares, J.J. Weis, and M.M. Telo da Gama, *Phys. Rev. E* **59**(1999) 4388.
 18. S. Cutillas and J. Liu, *Phys. Rev. E* **64** (2001) 011506.
 19. O. Volkova, S. Cutillas, and G. Bossis, *Phys. Rev. Lett.* **82** (1999) 233.
 20. X. Tang and H. Conrad, *J. Phys. D: Appl. Phys.* **33** (2000) 3026-3032.
 21. R. Tao and Q. Jiang, *Phys. Rev. E* **57** (1998) 5761.
 22. S. Cutillas, G. Bossis, and A. Cebers, *Phys. Rev. E* **57** (1998) 804.
 23. P. Domínguez-García, S. Melle, J.M. Pastor and M.A. Rubio, *Phys. Rev. E* **76** (2007) 051403.
 24. P. Domínguez-García, S. Melle, and M.A. Rubio, *J. Colloid Interface Sci.* **333** (2009) 221-229.
 25. F. Donado, U. Sandoval, and J.L. Carrillo, *Phys. Rev. E* **79** (2009) 011406.
 26. U. Sandoval, J.L. Carrillo, and F. Donado, *Rev. Mex. Fís. E* **56** (2010) 123-133.

27. B.J. de Gans, N.J. Duin, D. van den Ende, and J. Mellema, *J. Chem. Phys.* **113** (2000) 2032.
28. M.A. Osipov, P.I.C. Teixeira, and M.M. Telo da Gama, *Phys. Rev. E* **54** (1996) 2597.
29. J. Huang, P. Lai, *Physica A* **281** (2000) 105.